

A New Proposal to Jefferson Lab PAC48

Measurement of the Two-Photon Exchange contribution to the electron-neutron elastic scattering cross section

S. Alsalmi (spokesperson)

King Saud University, Riyadh 11451, Saudi Arabia

E. Fuchey (spokesperson) and A.J.R. Puckett*

University of Connecticut, Storrs, Connecticut 06269, USA

B. Wojtsekowski (spokesperson), S. Barcus*, A. Camsonne*, J-P. Chen*,
R. Ent*, D. Gaskell*, O. Hansen*, M. Jones*, C. Keppel*, D. Mack*,
D. Meekins*, R. Michaels*, B. Sawatzky*, G. Smith*, and S. Wood*

Thomas Jefferson National Accelerator Facility, Newport News, Virginia 23606, USA

J. Arrington* and P. Reimer*

Argonne National Laboratory, 9700 S Cass Ave, Lemont, Illinois 60439, USA

T. Averett*

The College of William and Mary, Williamsburg, Virginia 23185, USA

K. Aniol*

California State University, Los Angeles, CA 90032, USA

V. Bellini*

Istituto Nazionale di Fisica Nucleare, I-95123 Catania, Italy

W. Boeglin* and P. Markowitz*

Florida International University, Miami, FL 33199, USA

G. Cates*, K. Gnanvo*, C. Gu*, J. Liu*, N. Liyanage*,
 V. Nelyubin*, D. Nguyen*, and C. Palatchi*

University of Virginia, Charlottesville, Virginia 232904, USA

E. Cisbani*, F. Meddi*, and G. Urciuoli*

Istituto Nazionale di Fisica Nucleare - Sezione di Roma,

P.le Aldo Moro, 2 - 00185 Roma, Italy

J.C. Cornejo* and B. Quinn*

Carnegie Mellon University, Pittsburgh, Pennsylvania 15213, USA

B. Crowe* and B. Vlahovic*

North Carolina Central University, Durham, North Carolina 27707, USA

D. Hamilton* and R. Montgomery*

SUPA School of Physics and Astronomy,

University of Glasgow, Glasgow G12 8QQ, UK

F. Hauenstein*

Old Dominion University, Norfolk, Virginia 23529, USA

C. Petta* and C. Suttera*

Istituto Nazionale di Fisica Nucleare, Dipt. di Fisica dell Univ. di Catania, I-95123 Catania, Italy

G.G. Petratos*

Kent State University, Kent, OH 44242, USA

A. Sarty*

Saint Mary's University, Halifax, Nova Scotia B3H 3C3, Canada

K. Slifer*

University of New Hampshire, Durham, NH 03824, USA

A. Shahinyan*

AANL, 2 Alikhanian Brothers Street, 0036, Yerevan, Armenia

S. Širca*

Faculty of Mathematics and Physics, University of Ljubljana, 1000 Ljubljana, Slovenia

E. Voutier*

Institut de Physique Nucléaire, 15 Rue Georges Clemenceau, 91400 Orsay, France

(Dated: June 10, 2020)

Abstract

We propose make a high precision measurement of the two-photon exchange contribution (TPE) in elastic electron-neutron scattering at a four-momentum transfer $Q^2 = 4.5$ $(\text{GeV}/c)^2$. While significant efforts to study the two-photon-exchange have focused around elastic electron-proton scattering, the impact of TPE on neutron form factors was never examined experimentally. The proposed experiment will provide the very first assessment of the two-photon exchange in electron-neutron scattering, which will be important for understanding of the nucleon form factor physics.

The proposed experiment will be performed in Hall A using the BigBite (BB) spectrometer to detect the scattered electrons and the Super-BigBite (SBS) to detect the protons and neutrons. The experiment should run concurrently with the E12-09-019 G_M^n and E12-17-004 G_E^n -Recoil experiments, which are expected to run in 2021. The experimental setup of the proposed experiment will be identical to that of E12-09-019 experiment.

The “ratio” method will be used to extract the electric form factor of the neutron G_E^n by scattering unpolarized electrons from deuterium quasi-elastically at two beam energies 4.4 and 6.6 GeV and electron scattering angles 41.9 and 23.3 degrees respectively. In the proposed approach, systematic errors are greatly reduced compared to those in the traditional single electron arm configuration. Several experiments at Mainz and JLab have used the ratio method to measure the neutron magnetic form factor in the past years. The method can be extended to extract the neutron electric form factor even with less stringent requirements on the knowledge of the absolute neutron detection efficiency and experimental kinematics.

I. INTRODUCTION

In 1950's, a series of experiments performed by R. Hofstadter [1] revealed that the nucleons have a substructure (would be called later the quarks and gluons). The experiment confirmed M. Rosenbluth's theory [2] based on one-photon exchange approximation. In the Born approximation, where the interaction between the electron and the nucleon occurs *via* an exchange of a one virtual photon (OPE), the unpolarized $e - N$ elastic cross section can be expressed in terms of a nucleon magnetic, G_M , and electric, G_E , form factors. These form factors describe the deviation from a point-like scattering cross section:

$$\left(\frac{d\sigma}{d\Omega} \right)_{eN \rightarrow eN} = \frac{\sigma_{Mott}}{\epsilon(1 + \tau)} [\tau \cdot G_M^2(Q^2) + \epsilon \cdot G_E^2(Q^2)] = \sigma_T + \epsilon \cdot \sigma_L, \quad (1)$$

where E and E' are the incident and scattered electron energies, respectively, θ is the electron scattering angle, $\tau \equiv -q^2/4M^2$, with $-q^2 \equiv Q^2 = 4EE' \sin(\theta/2)$ being the negative four momentum transfer square, M is the nucleon mass, and $\epsilon = [1 + 2(1 + \tau) \tan^2(\theta/2)]^{-1}$ is the longitudinal polarization of the virtual photon, σ_L and σ_T are the cross sections for longitudinally and transversely polarized virtual photons, respectively.

The linear ϵ dependence of the cross section is due to σ_L term, see Eq. 1. The ratio σ_L/σ_T is a Rosenbluth slope related to G_E/G_M (in OPE), see Fig. 1. The data show that at Q^2 of 4-5 $(\text{GeV}/c)^2$ the Rosenbluth slope is three-four times larger than it suppose to be (in OPE) for the observed values of the G_E^p/G_M^p ratio.

The nucleon electromagnetic form factors can reveal a lot of information about the nucleon internal structure, as well as the quark distribution. The form factors depend only on one variable the negative square of the four-momentum transfer carried by the photon, Q^2 . In the limit of large Q^2 , pQCD provides well-motivated predictions for the Q^2 -dependance of the form factors and their ratio. However, it was never predicted at what Q^2 range the pQCD prediction (scaling) will be valid. Studies of GPDs show that pQCD validity will require a very large Q^2 of 100 $(\text{GeV}/c)^2$. It was discovered at JLab, using the double polarization methods, that the proton electric and magnetic form factors behave differently starting at

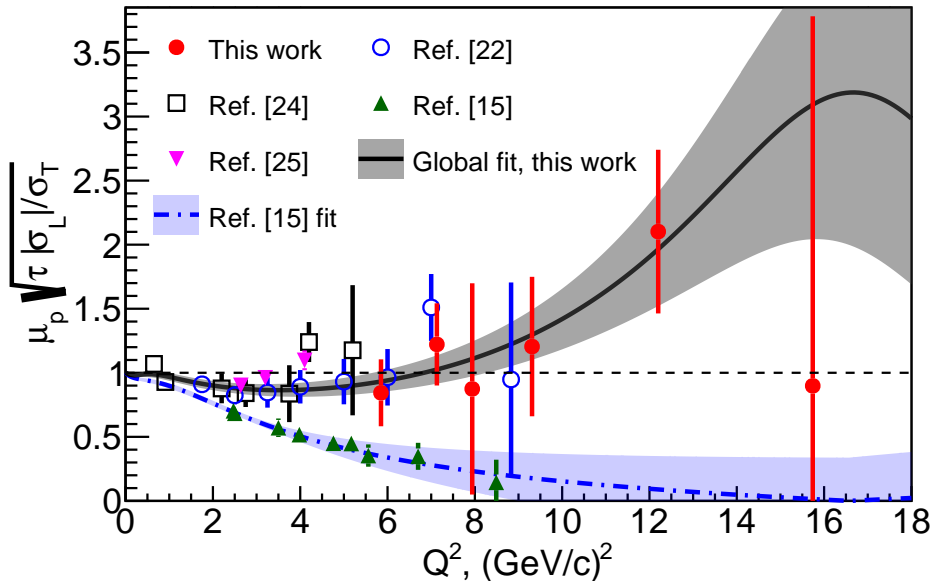


FIG. 1. The square root of Rosenbluth slope, corrected for kinematical factor $\sqrt{\tau}$ and μ_p , observed in elastic electron-proton scattering, adopted from Ref. [3].

²⁷ $Q^2 \approx 1 \text{ (GeV/c)}^2$.

²⁸ Experimentally, the nucleon form factors can be measured using one of two techniques:
²⁹ polarization transfer technique and Rosenbluth technique. The polarization method exam-
³⁰ ines the polarization transfer from longitudinally polarized electron to the recoiling nucleon
³¹ and determine the resulting azimuthal asymmetry distribution using a polarimeter. Alter-
³² natively, one can use the polarized electron beam and a polarized target. While in the
³³ Rosenbluth method, the electric and magnetic form factors can be separated by making
³⁴ two or more measurements with different ϵ values (*i.e.* different beam energies and angles),
³⁵ but with same Q^2 value. Rosenbluth technique requires an accurate measurement of the
³⁶ cross section and suffers from large systematic uncertainties arising from several factors. For
³⁷ instance, an accurate knowledge of the neutron detector efficiency is required.

³⁸ When comparing the values of G_E^p/G_M^p obtained from both techniques, a significant dis-
³⁹ crepancy was observed (see Fig. 1). Such discrepancy implies a potential problem in our
⁴⁰ understanding of the nucleon substructure. Many efforts were made in order to provide
⁴¹ legitimate explanation, and it is believed that the inconsistency is due to contribution of

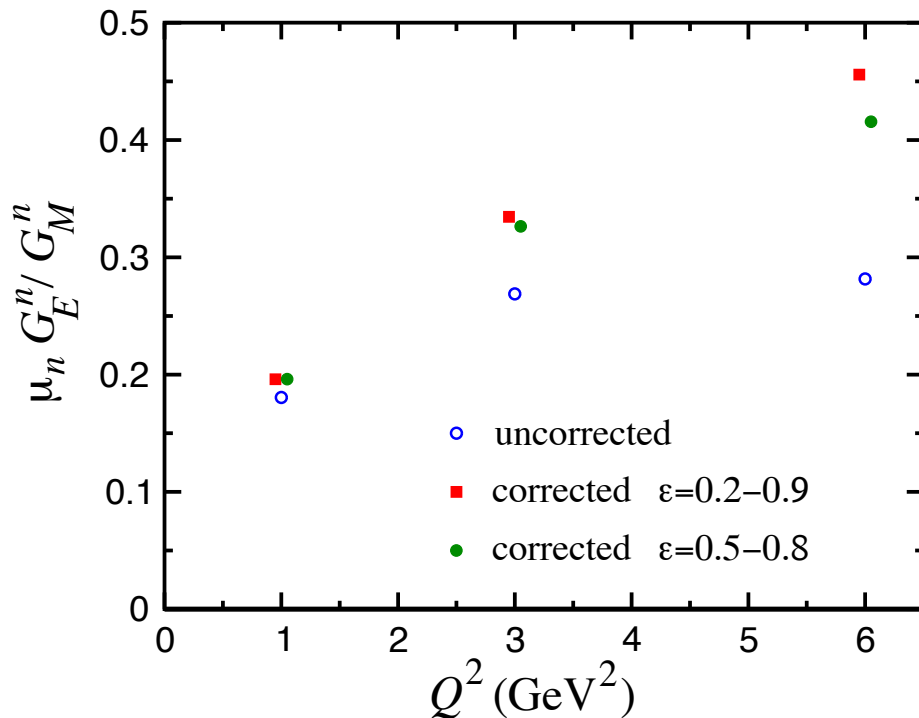


FIG. 2. Projected impact of TPE on G_E^n/G_M^n using LT separation, according to Ref. [4].

42 two-photon exchange in $e - N$ elastic scattering process, see Refs. [5, 6]. Predictions made
 43 for the neutron case are shown in Fig. 2 , adopted from [4]. The contribution of TPE could
 44 reach about 30% of Rosenbluth slope value at 5 (GeV/c) 2 .

45 In the following we propose to make precision L/T separation of the elastic electron-
 46 neutron cross section and first experimental assessment of the two-photon exchange contri-
 47 bution on the neutron magnetic form factor measurements (see also Ref. [7]). The result of
 48 the nTPE experiment will likely add a new component to our understanding of the elastic
 49 electron-nucleon process.

50

II. PHYSICS MOTIVATION

51 The nucleon plays the same central role in hadronic physics that the hydrogen atom does
 52 in atomic physics and the deuteron in the physics of nuclei. The structure of the nucleon
 53 and its specific properties, such as charge, magnetic moment, size, mass; the elastic electron
 54 scattering form factors, resonances; and structure functions in DIS, are of fundamental sci-
 55 entific interest. The isospin is a fundamental property of the nucleon, so both the proton and
 56 neutron investigations are important to do. By using data on the proton and neutron form
 57 factors the flavour structure could be explored [8]. It is already provided the most direct
 58 evidence for a diquark correlation in the nucleon [9–11].

59 Hadron structure, as seen in elastic electron scattering, in one-photon approximation,
 60 defined by two functions of four momentum transfer square. They are: the helicity conserving
 61 Dirac form factor, F_1 , which describes the distribution of the electric charge, and the helicity
 62 non-conserving Pauli form factor, F_2 , describes the distribution of the magnetic moment.
 63 These two form factors are the ingredients of the hadronic current. These form factors
 64 contain information on the transverse charge distribution for an unpolarized and transversely
 65 polarized nucleon, respectively, in the infinite momentum frame [12, 13].

66 The Sachs form factors, G_E and G_M , the ratio of which will be extracted directly from
 67 the data, are related to F_1 and F_2 by

$$F_1 = \frac{G_E + \tau G_M}{1 + \tau} \text{ and } F_2 = \frac{G_M - G_E}{\kappa(1 + \tau)}, \quad (2)$$

68 where κ is the nucleon anomalous magnetic moment.

69 Already twenty four years ago, important developments in QCD phenomenology has
 70 been the exploration of the generalized parton distribution (GPD) formalism [14–16], which
 71 provides relations between inclusive and exclusive observables. The nucleon elastic form
 72 factors F_1 and F_2 are given by the first moments of the GPDs

$$F_1(t) = \sum_q \int_0^1 H^q(x, \xi, t, \mu) dx \text{ and } F_2(t) = \sum_q \int_0^1 E^q(x, \xi, t, \mu) dx, \quad (3)$$

73 where H^q and E^q are two of the generalized parton distributions, x is the standard Bjorken
 74 x , ξ is the “skewness” of the reaction, t is the four-momentum transferred by the electron,

⁷⁵ μ is a scale parameter necessary from the evolution over Q^2 , analogous to DIS parton distributions, and the sum is over all quarks and anti-quarks. These may be accessed through processes such as deeply virtual Compton scattering, where the interaction is factorized into a hard part with the virtual photon/photon interactions with an individual quark and a soft part of the residual system where the GPD information is contained.

⁸⁰ Fundamental nucleon feature, the spin, is related to GPDs, as shown by X. Ji [15]. The moments of GPDs can yield information, according to the Ji's Angular Momentum Sum Rule, on the contribution to the nucleon spin from quarks and gluons, including both the quark spin and orbital angular momentum.

⁸⁴ At present, experimental measurements of GPDs are still scarce. Until high Q^2 DVCS data becomes available, work has been done to attempt to parameterize these GPDs, which rely heavily on data from electromagnetic form factors and parton distributions from DIS as constraints [17]. Data at high Q^2 for G_E^n would contribute significantly in the development of these models.

⁸⁹ As we presented above the form factors are important components for GPDs development. However, the cross section of elastic $e-p$ scattering contains a significant contribution to σ_L , which at high Q^2 is much larger than theory calculations expected [18]. Such an alarming observation underlines that understanding of TPE effect is essential for hadron physics.

93

III. TECHNIQUE

94 The neutron form factors are challenging to be determine experimentally especially be-
 95 cause there is no free neutron target. However, since the deuterium is a loosely coupled
 96 system, it can be viewed as the sum of a proton target and a neutron target. In fact, quasi-
 97 elastic scattering from deuterium has been used to extract the neutron magnetic form factor,
 98 G_M^n , at modestly high Q^2 for decades [19, 20] in the single arm (e, e') experiments. How-
 99 ever, the proton cross section needs to be subtracted by applying a single-arm quasi-elastic
 100 electron-proton scattering. This “proton-subtraction” technique suffers from a number sys-
 101 tematic uncertainties e.g. contributions from inelastic and secondary scattering processes.

102 Many year ago, L. Durand [21] proposed the so-called “ratio-method” based on the mea-
 103 surement of both $D(e, e'n)$ and $D(e, e'p)$ reactions. In this method, many of the systematic
 104 errors are cancel out. Several experiments [22–24] have applied the ratio-method to determine
 105 the neutron magnetic form factor. We propose to use this method to measure Rosenbluth
 106 slope and extract (in OPE approximation) the neutron electric form factor, G_E^n .

107 Data will be collected for quasi-elastic electron scattering from deuteron in process
 108 $D(e, e'n)p$. A complementary $D(e, e'p)n$ data will be taken to calibrate the experiment ap-
 109 paratus. The current knowledge of the $e - p$ elastic scattering cross section (obtained in the
 110 single arm $H(e, e')p$ and $H(e, p)e'$ experiments) will be also used for precision determination
 111 the experiment kinematics.

112 Applying Rosenbluth technique to measure G_E^n requires accurate measurement of the cross
 113 section and suffers from large uncertainties. To overcome this issue, we propose to extract
 114 the value of G_E^n from the measured the ratio of quasi-elastic yields, $R_{n/p}$, in scattering from
 115 a deuteron target as follows:

$$R_{n/p} \equiv R_{observed} = \frac{N_{e, e'n}}{N_{e, e'p}} \quad (4)$$

116 $R_{observed}$ needs to be corrected to extract the ratio of e-n/e-p scattering from nucleons:

$$R_{corrected} = f_{corr} \times R_{observed} , \quad (5)$$

117 where the correction factor $f_{correction}$ takes into account the variation in the hadron efficiencies
 118 due to changes of $e - N$ Jacobian, the radiative corrections, and absorption in path from the
 119 target to the detector, and small re-scattering correction.

120 In one-photon approximation, $R_{corrected}$ can be presented as:

$$R_{corrected} = \frac{\sigma_{Mott}^n \cdot (1 + \tau_p)}{\sigma_{Mott}^p \cdot (1 + \tau_n)} \times \frac{\epsilon \sigma_L^n + \sigma_T^n}{\epsilon \sigma_L^p + \sigma_T^p} \quad (6)$$

It is important that the ratio $R_{Mott} = \frac{\sigma_{Mott}^n \cdot (1 + \tau_p)}{\sigma_{Mott}^p \cdot (1 + \tau_n)}$ could be determined with very high relative accuracy even with modest precision for the beam energy, electron scattering angle, and detector solid angle. Now, let us write the $R_{corrected}$ at two values of ϵ using $R_c^{n(p)} = \sigma_L^{n(p)} / \sigma_T^{n(p)}$ as:

$$R_{corrected,\epsilon_1} = R_{Mott,\epsilon_1} \times \frac{\epsilon_1 \sigma_L^n + \sigma_T^n}{\epsilon_1 \sigma_L^p + \sigma_T^p} \quad R_{corrected,\epsilon_2} = R_{Mott,\epsilon_2} \times \frac{\epsilon_2 \sigma_L^n + \sigma_T^n}{\epsilon_2 \sigma_L^p + \sigma_T^p}$$

In these two equations there are two unknown variables: σ_L^n and σ_T^n . The dominant contribution to the uncertainty of the slope of the cross section vs. ϵ , $S_c^n = \sigma_L^n / \sigma_T^n$, will come from the uncertainty of S_c^p . At $Q^2=4.5$ (GeV/c)², according to the global analysis of $e - p$ cross section [3], the value of S_c^p is close to $1/(\tau \mu_p^2) = 0.107$ with uncertainty of 0.01. The resulting equation for S_c^n is:

$$A = B \times \frac{1 + \epsilon_1 S_c^n}{1 + \epsilon_2 S_c^n} \approx B \times (1 + \Delta \epsilon \cdot S_c^n),$$

121 where the variable $A = R_{corrected,\epsilon_1} / R_{corrected,\epsilon_2}$ will be measured with relative precision of
 122 0.1%. Assuming, for this estimate, equal values of Q^2 for two kinematics, the τ and σ_T for
 123 two kinematics are canceled out, and the variable $B = R_{Mott,\epsilon_1} / R_{Mott,\epsilon_2} \times (1 + \epsilon_2 S_c^p) / (1 + \epsilon_1 S_c^p)$.
 124 For actual small range of ϵ and small value of the slope, the $B \approx (1 - \Delta \epsilon \cdot S_c^p)$. The value
 125 of B will be determined from global proton $e - p$ data to a precision of 0.25×0.01 .

126 At $Q^2=4.5$ (GeV/c)² the ratio $\mu_n G_E^n / G_M^n$ is of 0.55 ± 0.05 , see the review [25]. In a
 127 simplest model, the slope S_c^n is a sum of the slope due to G_E^n / G_M^n and the TPE contribution.
 128 If we use for TPE the prediction [4], shown in Fig. 2, the TPE leads to increase of S_c^n by a
 129 factor of 2, so the result of this experiment for TPE will be $0.069 \pm 0.012 \pm 0.01$, where the
 130 first uncertainty is due to accuracy of G_E^n / G_M^n and the second one due to projected precision
 131 of this experiment. It would be a 4-4.5 sigma observation of the neutron TPE.

132

IV. EXPERIMENTAL SETUP

133 As illustrated in Fig. 3, this experiment will study electron scattering from a 15 cm
 134 long liquid Deuterium target held in a vacuum. The scattered electron will be detected
 135 in the BigBite spectrometer with an upgraded electron detector stack. The neutron arm is
 136 arranged with a dipole magnet 48D48 (SBS) and a segmented hadron calorimeter HCAL. The
 137 whole detector package was designed and is now under assembling for the GMn, E12-09-019,
 138 experiment.

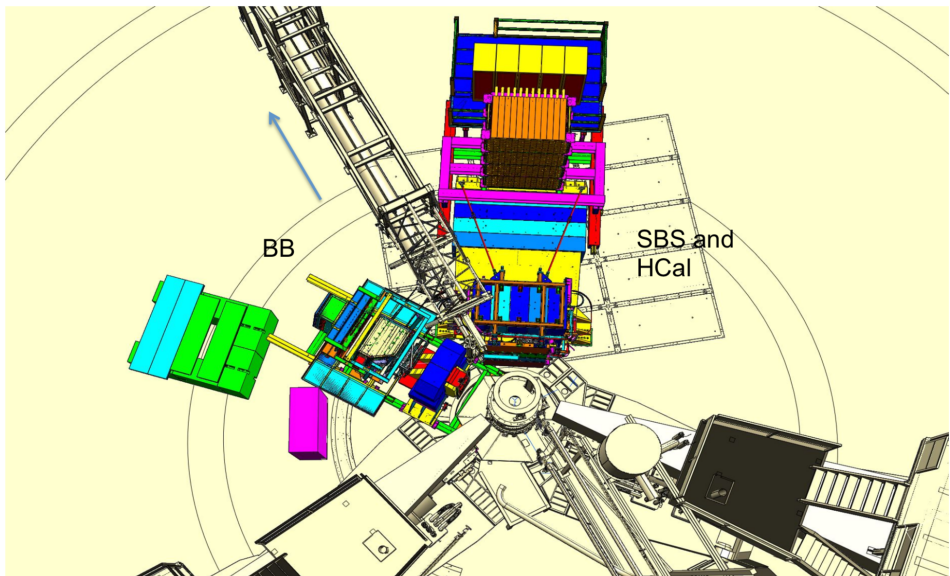


FIG. 3. Layout of the experimental setup in nTPE.

139

1. Parameters of the SBS

140 The 48D48 magnet from Brookhaven was acquired as part of the Super Bigbite project
 141 and will be available for this experiment. It consists of a large dipole magnet which provides
 142 a field integral of about $1.7 \text{ T} \cdot \text{m}$, allowing for quasielastic protons to be sufficiently deflected
 143 to allow clear differentiation from neutrons. The active field volume has an opening of $46 \times$
 144 $25 \text{ vertical} \times \text{horizontal}$), matching the aspect ratio of the neutron arm, and a depth of 48
 145 cm.

¹⁴⁶ The placement of this magnet will be 1.6 m away from the target, which would normally
¹⁴⁷ interfere with the beamline. To accommodate this, modifications were made to the iron yoke
¹⁴⁸ such that the beamline will pass through the magnet yoke area.

¹⁴⁹ The field configuration will be such that positively charged particles will be deflected
¹⁵⁰ upwards away from the hall floor. For a field integral of 1.7 Tesla-m, protons of momentum
¹⁵¹ 2.5 GeV/c will be deflected 250 mrad, which translates to a displacement of xxm. Including
¹⁵² expected detector resolution, the $p_{miss,\perp}$ distribution will be similar to what was seen in
¹⁵³ E02-013, so cuts of < 100 MeV/c will be appropriate. Monte Carlo simulations show a
¹⁵⁴ contamination of charged quasielastics to be negligible.

¹⁵⁵ The presence of the magnet also works to sweep low energy charged particles from the
¹⁵⁶ target away from the neutron arm. Particles of momentum less than 1.3 GeV/c will be
¹⁵⁷ entirely swept outside of the neutron arm acceptance. This greatly reduces the amount of
¹⁵⁸ charged low energy background.

159

A. The BigBite Spectrometer

160 Scattered electrons will be detected in the BigBite spectrometer. The spectrometer con-
 161 sists of a single dipole magnet (with magnetic field approximately 1.2 Tesla-m and a detection
 162 system, see Fig. 4.

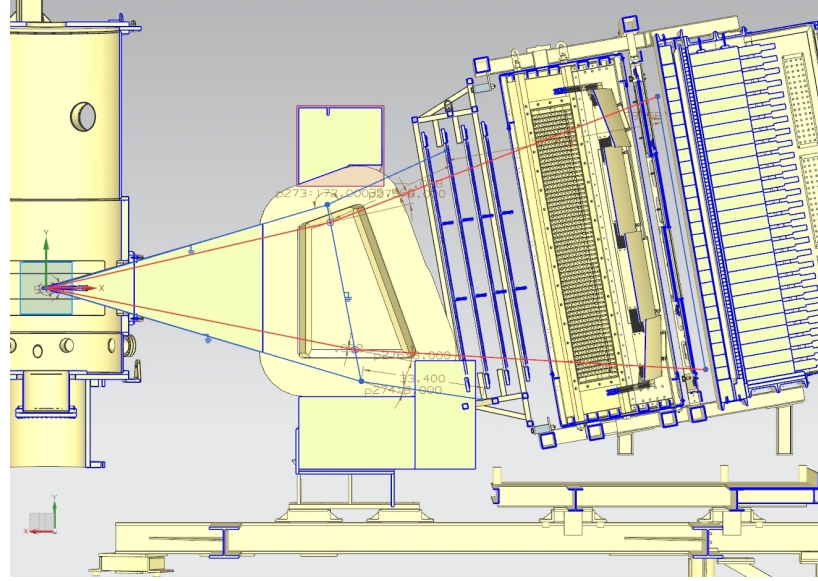


FIG. 4. The BigBite spectrometer with the upgraded detector stack.

163

1. Simulation of BigBite

164

2. Detector Package

- 165 a. Background Rate in BigBite
- 166 b. Front GEM chambers
- 167 c. Gas Cherenkov Counter
- 168 d. Rear GEM chamber
- 169 e. Shower and Preshower
- 170 f. Timing Scintillator Hodoscope

171

3. Trigger

172

4. Simulation of BigBite

173

a. Rates in the detectors

174

b. Trigger rate and efficiency

175

B. Neutron Detector

176 S

177 *1. Structure of the Neutron Detector*

178 **V. SIMULATIONS, ESTIMATIONS OF COUNTING RATES AND**
 179 **ACCIDENTALS**

180 The estimations of counting rates accidentals have been performed using G4SBS, the
 181 GEANT4-based simulation package developed for the SBS experiment [?]. This package
 182 includes a wide range of event generators, which allows to evaluate the rates for both events
 183 of interest (signal) and background. The representation of the experiment apparatus in
 184 G4SBS is shown in the high ϵ configuration on Fig. 5.

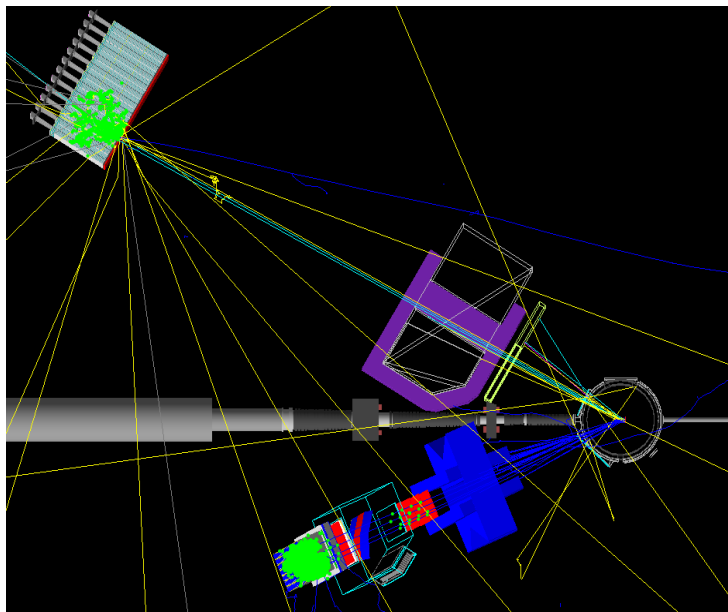


FIG. 5. Top view of the experimental apparatus model in G4SBS, shown in the high ϵ configuration. The beam direction is indicated, as well as the main elements (HCAL, SBS magnet, BigBite spectrometer)

185
 186

187 **A. Quasi-elastic counting rates**

188 The signals for this experiment have been generated using the G4SBS elastic/quasi-elastic
 189 generator. We generated 1M events sample for each kinematics, on a solid angle that was

¹⁹⁰ larger than the detector acceptance. To evaluate the detector solid angle, we define simple
¹⁹¹ criteria that each event has to pass, defined as the following;

- ¹⁹² • require a primary track, going through all 5 GEM layers (electron arm);
- ¹⁹³ • require non-zero energy deposit in both the preshower and shower (electron arm);
- ¹⁹⁴ • require non-zero energy deposit in HCal (hadron arm).

¹⁹⁵ The detector solid angle, for both proton and neutron, are defined in Table. I

Point (ϵ)	$\Delta\Omega_e$ (msr)	$\Delta\Omega_e \otimes \Delta\Omega_n$ (msr)	$\Delta\Omega_e \otimes \Delta\Omega_p$ (msr)
1 (0.599)	52.4	46.7	47.2
2 (0.838)	32.7	23.4	23.0

TABLE I. Kinematics solid angles and efficiencies.

¹⁹⁶

¹⁹⁷ Then, we evaluate the detection efficiency. For the electron, we require the energy recon-
¹⁹⁸ structed in the BigBite calorimeter to be above a threshold defined as $thr = \mu_E - 2.5 * \sigma_E$,
¹⁹⁹ as well as a minimum number of GRINCH PMTs fired due to the primary electron; For
²⁰⁰ HCal, we require the threshold to be such as we obtain 90% efficiency. These values are
²⁰¹ summarized in Table. II.

Point (ϵ)	BB thr. (GeV)	HCal thr. (GeV)	η_e	η_n	η_p
1 (0.599)	1.32	1.06	0.902	0.904	0.892
2 (0.838)	2.99	0.09	0.807	0.887	0.876

TABLE II. Kinematics solid angles and efficiencies.

²⁰²

203 The counting rates are evaluated using the events that have passed the selection described
 204 above, and weighting those events with the cross section calculated by G4SBS, multiplied
 205 by the generation solid angle, using the formula:

$$N_{est} = \mathcal{L}\Delta t \times \sum_{i \in acc\ evts} \frac{d\sigma}{d\Omega} * \Delta\Omega_{Gen}/N_{Gen} \quad (7)$$

206 The counting rates for both kinematics are available in Table. III, assuming 12 hours of
 207 running at an intensity of $30 \mu\text{A}$ on a 15cm liquid deuterium target, with density 0.169
 208 g.cm^{-3} .

Point (ϵ)	QE $e-n$ counts	QE $e-p$ counts	F_n^2 ($\times 10^{-3}$)	ΔF_n^2 ($\times 10^{-6}$)	F_p^2 ($\times 10^{-3}$)	ΔF_p^2 ($\times 10^{-6}$)
1 (0.599)	1.68×10^6	4.57×10^6	1.09	0.84	2.97	1.39
2 (0.838)	4.52×10^6	1.21×10^7	0.92	0.43	2.53	0.79

TABLE III. Quasi-elastic counting rates, and “reduced cross section” as defined by Eq. ???. These rates assume 12 hours of running at an intensity of $30 \mu\text{A}$ on a 15cm liquid deuterium target, with density 0.169 g.cm^{-3} .

209

210 The calculation of the F_2 term requires the evaluation of the Mott cross section. The
 211 Mott cross section has been calculated with the weighted average of the electron variables
 212 (momentum and polar angle).

Point (ϵ)	$\langle \theta_e \rangle$ (deg)	$\langle k' \rangle$ (GeV)	$\langle Q^2 \rangle$ (GeV 2)	σ_{Mott} (nb sr $^{-1}$)
1 (0.599)	41.7	2.01	4.47	6.62
2 (0.838)	22.9	4.26	4.40	48.0

TABLE IV. Cross-section weighted average of kinematic variables over the BigBite acceptance.
 The Mott cross section has been evaluated at these values.

213

214

B. Background and trigger rates

215 The main processes expected to contribute the trigger rates for the BigBite spectrometer
 216 are:

- 217 • the inelastic electron nucleon scattering process;
- 218 • photons from inclusive π^0 production;
- 219 • and to a lesser extent, charged pions.

220 One the other hand, we expect all sorts of hadronic backgrounds to contribute to the rates in
 221 HCal, the dominant ones being pions. Both the inelastic scattering and the inclusive neutral
 222 and charged pion production are implemented in G4SBS, the latter relying on the Wiser
 223 parametrization [?]. We may also considered the minimum-bias “beam-on-target” gener-
 224 ator for the HCal background, especially at lower angle (all electromagnetic and hadronic
 225 processes being built-in in G4SBS).

226 The thresholds to apply to each arm are determined as a function of the elastic peak. For
 227 the electron arm, the threshold has been set at $\mu_E - 2.5\sigma_E$, μ_E and σ_E being respectively
 228 the position and width of the fitted elastic peak. Fig. 6 presents the distributions of rate of
 229 energy deposit for the different processes involved in the BigBite trigger rates.

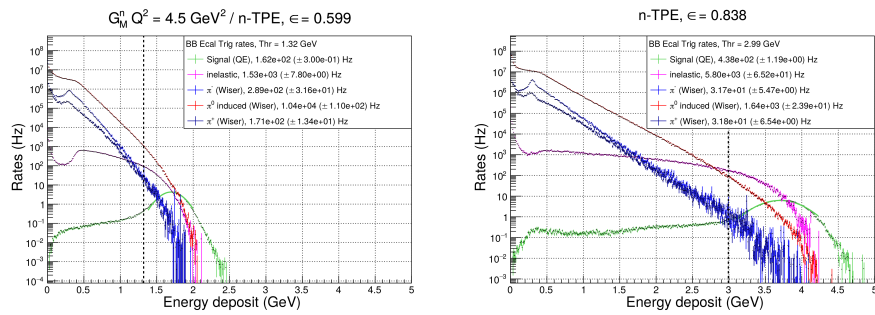


FIG. 6. Rates of the different process contributing to the BigBite electron arm trigger, for the low ϵ (left) and the high ϵ (right). Quasi-elastic is in green, inelastic in magenta, π^0 in red, π^- in blue, and π^+ in dark blue. Note the resolution for the elastic peak in the BigBite shower is ~ 0.3 GeV.

230

231

232 Since HCal is a sampling calorimeter (meaning that only a fraction of the shower energy
 233 is measured), it's resolution is significantly wider (~ 0.7 GeV). Due to this, the threshold
 234 is at 90% efficiency (which corresponds to ~ 0.1 GeV for both kinematics. Fig. ?? presents
 235 the distributions of rate of energy deposit for the different processes involved in the BigBite
 236 trigger rates.

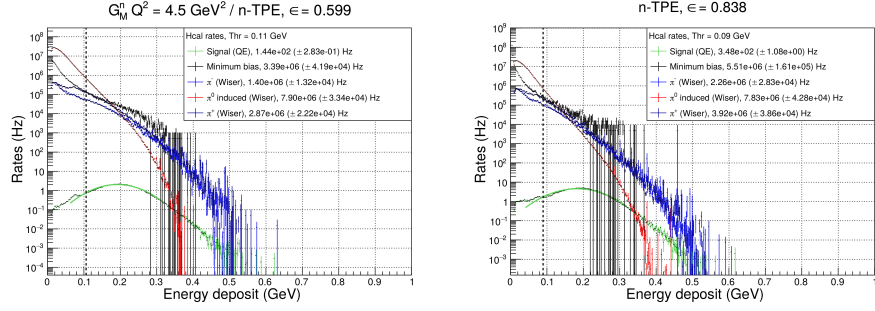


FIG. 7. Rates of the different process contributing to the HCal trigger, for the low ϵ (left) and the high ϵ (right). Quasi-elastic is in green, minimum bias in black, π^0 in red, π^- in blue, and π^+ in dark blue. Note the peak itself is around 0.2 GeV for 3.2 GeV nucleons.

237
 238
 239 The thresholds and trigger rates for each arm, as well as the coincidence rate (assuming
 240 30ns coincidence window), are summarized in Table. ??.

241
 242 Note that for HCal, the “total rates” is either the sum of inclusive charged and neutral pions
 243 evaluated with the Wiser cross sections *or* the “minimum bias” beam on target. We have
 244 good reasons to think that the Wiser code results actually overestimate the HCal rates, but
 245 for the sake of thoroughness, we have checked the coincidence rates assuming the sum of the
 246 inclusive pions (evaluated with the Wiser cross sections) as the HCal rates.

247 In the worst case scenario, the coincidence rates could be as high as 5kHz, which might be
 248 at the limit of manageability for the DAQ. However, a slight increase on the HCal threshold
 249 (which would drop the efficiency from $\sim 90\%$ to $\sim 85\%$) would decrease the total HCal rates by
 250 $\sim 35\%$ to 40% in this worst case scenario, which would make the situation more manageable
 251 (3.3 kHz).

Point (ϵ)	1 (0.599)		2 (0.838)	
	BigBite rates (Hz)	HCal rates (Hz)	BigBite rates (Hz)	HCal rates (Hz)
threshold (GeV)	1.32	0.106	2.99	0.090
Quasi-elastic	1.62×10^2	1.44×10^2	4.38×10^2	3.48×10^2
Inelastic	1.62×10^3	-	5.80×10^3	-
π^0 (Wiser)	3.16×10^2	1.40×10^6	3.17×10^2	2.26×10^6
π^+ (Wiser)	1.16×10^4	7.90×10^6	1.64×10^3	7.83×10^6
π^- (Wiser)	1.84×10^2	2.87×10^6	3.18×10^2	3.92×10^6
Minimum bias	-	3.39×10^6	-	5.40×10^6 (*)
<i>Total</i>	1.39×10^4	1.22×10^7	8.51×10^3	1.40×10^7
(min. bias - HCal only)		/ 3.39×10^6		/ 5.40×10^6
Coincidence rate	5.09×10^3		3.57×10^3	
(with min. bias HCal)	1.41×10^3		1.38×10^3	

TABLE V. Trigger rates for BigBite and HCal, with the different process contributions separated, and the sum. For HCal, the total rates is either the sum of the (Wiser) inclusive pions or the minimum bias. The coincidence rates assume a 30 ns coincidence window.

252

VI. PROPOSED MEASUREMENTS

253 We propose to use the same experimental setup of E12-09-019 experiment. We will add
 254 a kinematic point at $Q^2 = 4.5 \text{ (GeV/c)}^2$, but with a higher ϵ value. This additional point
 255 along with the data point of E12-09-019 experiment will allow us to perform LT separation
 256 and obtain (in one-photon approximation) the G_E^n value. Table 1 displays the kinematic
 257 setting of the proposed experiment.

Point	Q^2 (GeV/c) 2	E (GeV)	E' (GeV)	θ_{BB} degrees	θ_{SBS} degrees	ϵ (%)	$\Delta\sigma$ (%)	ΔTPE (%)
1	4.5	4.4	2.0	41.88	24.67	0.599		
2	4.5	6.6	4.2	23.23	31.2	0.838		

TABLE VI. Kinematic settings of the proposed experiment. The blue row is a kinematic point of E12-09-019 experiment.

258

259

VII. BEAM TIME REQUEST

260 **We request 48 hours total time (32 hours of beam-on target)** to measure the
 261 two-photon effect (and G_E^n in one-photon approximation) at $Q^2 = 4.5$ (GeV/c)² through a
 262 measurement of the cross sections of the reaction D(e,e'N) at a large value of the virtual
 263 photon polarization $\epsilon=0.84$. This experiment will take place in Hall A, utilizing the Big-
 264 Bite spectrometer to detect electrons scattered off the liquid deuterium target, and HCal
 265 calorimeter to detect the recoiling neutron and proton.

266 Data taking (if approved by PAC48) will take place in summer 2021 during the approved
 267 and scheduled run of the GMn, E12-09-019, experiment, which is going to measure the $e - n$
 268 elastic scattering cross section at $Q^2 = 4.5$ (GeV/c)² at $\epsilon=0.60$.

269 The set of instrumentation and required beam current for proposed measurement is iden-
 270 tical to one in the GMn experiment. The beam energy of 6.6 GeV will be used. One of two
 271 data points required for the cross section LT separation is already in the data taking plan of
 272 GMn.

273 There are no other measurements of TPE in the $e - n$ elastic scattering and knowledge
 274 of the TPE is essential for the understanding of the elastic electron scattering from neutron
 275 (and proton) and hadron structure. Furthermore, it is a necessary input in the analysis and
 276 interpretation of a wide range of electron scattering processes.

277 The kinematics of our measurements emphasize the same Q^2 range where TPE in $e - p$
 278 elastic scattering was observed to dominate in Rosenbluth slope. Measuring at this high
 279 momentum transfers will provide unique input for testing TPE calculations [4].

280 We propose to measure the Rosenbluth slope and extract (in one-photon approximation)
 281 $\delta G_E^n / G_M^n$ to an accuracy of 0.15, which would bring its precision to a level comparable with
 282 that of the double polarization experiments GEN-RP and GEN-He3 at such value of Q^2 .
 283 Such precision should be sufficient to detect the TPE contribution to the $e - n$ Rosenbluth
 284 slope on the three sigma level.

-
- 285 [1] R. Hofstadter, *Rev. Mod. Phys.* **28**, 214 (1956).
- 286 [2] M. N. Rosenbluth, *Phys. Rev.* **79**, 615 (1950).
- 287 [3] E. Christy *et al.*, “Two-photon exchange in electron-proton elastic scattering at large four-momentum transfer,” (2020), in preparation for publication in PRL.
- 288
- 289 [4] P. G. Blunden, W. Melnitchouk, and J. A. Tjon, *Phys. Rev.* **C72**, 034612 (2005), arXiv:nucl-th/0506039 [nucl-th].
- 290
- 291 [5] J. Arrington, P. G. Blunden, and W. Melnitchouk, *Prog. Part. Nucl. Phys.* **66**, 782 (2011), arXiv:1105.0951 [nucl-th].
- 292
- 293 [6] A. Afanasev, P. Blunden, D. Hasell, and B. Raue, *Prog. Part. Nucl. Phys.* **95**, 245 (2017), arXiv:1703.03874 [nucl-ex].
- 294
- 295 [7] B. Wojtsekhowski, in *Exclusive processes at high momentum transfer. Proceedings, Newport News, USA, May 15-18, 2002* (2002) arXiv:1706.02747 [physics.ins-det].
- 296
- 297 [8] G. D. Cates, C. W. de Jager, S. Riordan, and B. Wojtsekhowski, *Phys. Rev. Lett.* **106**, 252003 (2011), arXiv:1103.1808 [nucl-ex].
- 298
- 299 [9] C. D. Roberts, M. S. Bhagwat, A. Holl, and S. V. Wright, *Eur. Phys. J. ST* **140**, 53 (2007), arXiv:0802.0217 [nucl-th].
- 300
- 301 [10] J. Segovia, I. C. Cloet, C. D. Roberts, and S. M. Schmidt, *Few Body Syst.* **55**, 1185 (2014), arXiv:1408.2919 [nucl-th].
- 302
- 303 [11] B. Wojtsekhowski (2020) arXiv:2001.02190 [nucl-ex].
- 304 [12] G. A. Miller, *Phys. Rev. Lett.* **99**, 112001 (2007), arXiv:0705.2409 [nucl-th].
- 305 [13] C. E. Carlson and M. Vanderhaeghen, *Phys. Rev. Lett.* **100**, 032004 (2008), arXiv:0710.0835 [hep-ph].
- 306
- 307 [14] D. Muller, D. Robaschik, B. Geyer, F. M. Dittes, and J. Horejsi, *Fortsch. Phys.* **42**, 101 (1994), arXiv:hep-ph/9812448 [hep-ph].
- 308
- 309 [15] X.-D. Ji, *Phys. Rev. Lett.* **78**, 610 (1997), arXiv:hep-ph/9603249 [hep-ph].
- 310 [16] A. V. Radyushkin, *Phys. Lett.* **B380**, 417 (1996), arXiv:hep-ph/9604317 [hep-ph].

- ³¹¹ [17] M. Diehl and P. Kroll, *Eur. Phys. J.* **C73**, 2397 (2013), arXiv:1302.4604 [hep-ph].
- ³¹² [18] N. Kivel, “private communications,” (2020).
- ³¹³ [19] E. B. Hughes, T. A. Griffy, M. R. Yearian, and R. Hofstadter, *Phys. Rev.* **139**, B458 (1965).
- ³¹⁴ [20] R. G. Arnold *et al.*, *Phys. Rev. Lett.* **61**, 806 (1988).
- ³¹⁵ [21] L. Durand, *Phys. Rev.* **115**, 1020 (1959).
- ³¹⁶ [22] E. E. W. Bruins *et al.*, *Phys. Rev. Lett.* **75**, 21 (1995).
- ³¹⁷ [23] G. Kubon *et al.*, *Phys. Lett.* **B524**, 26 (2002), arXiv:nucl-ex/0107016 [nucl-ex].
- ³¹⁸ [24] J. Lachniet *et al.* (CLAS), *Phys. Rev. Lett.* **102**, 192001 (2009), arXiv:0811.1716 [nucl-ex].
- ³¹⁹ [25] V. Punjabi, C. F. Perdrisat, M. K. Jones, E. J. Brash, and C. E. Carlson, *Eur. Phys. J.* **A51**, 79 (2015), arXiv:1503.01452 [nucl-ex].
- ³²⁰